Electronic Supplementary Information

Gas-phase Negative Ion Photoelectron Spectroscopy and Reactivity of Phenylacetylide $PhCC^-$

Howard Z. Ma,[a] Wenjin Cao,[b] Yufei Xie,[a] Xue-Bin Wang,[b*] Richard A. J. O'Hair[a*]

a) School of Chemistry and Bio21 Molecular Science and Biotechnology Institute, University of Melbourne, 30 Flemington Rd, Parkville, Victoria, 3010, Australia.
b) Physical Sciences Division, Pacific Northwest National Laboratory, Richland, Washington 99352, United States.

Table S1 Experimental absolute rate constants for the ion-molecule reaction of Br- with CH_3I compared with literature values obtained *via* different instrumentation.

Method/Instrumentation	**Measured rate k_{expt} ($\times 10^{-11}$ cm^3 molecule^{-1} s^{-1})**
Flowing afterglow	2.89
LCQ	2.70
Linear ion trap*	2.87

* Present work

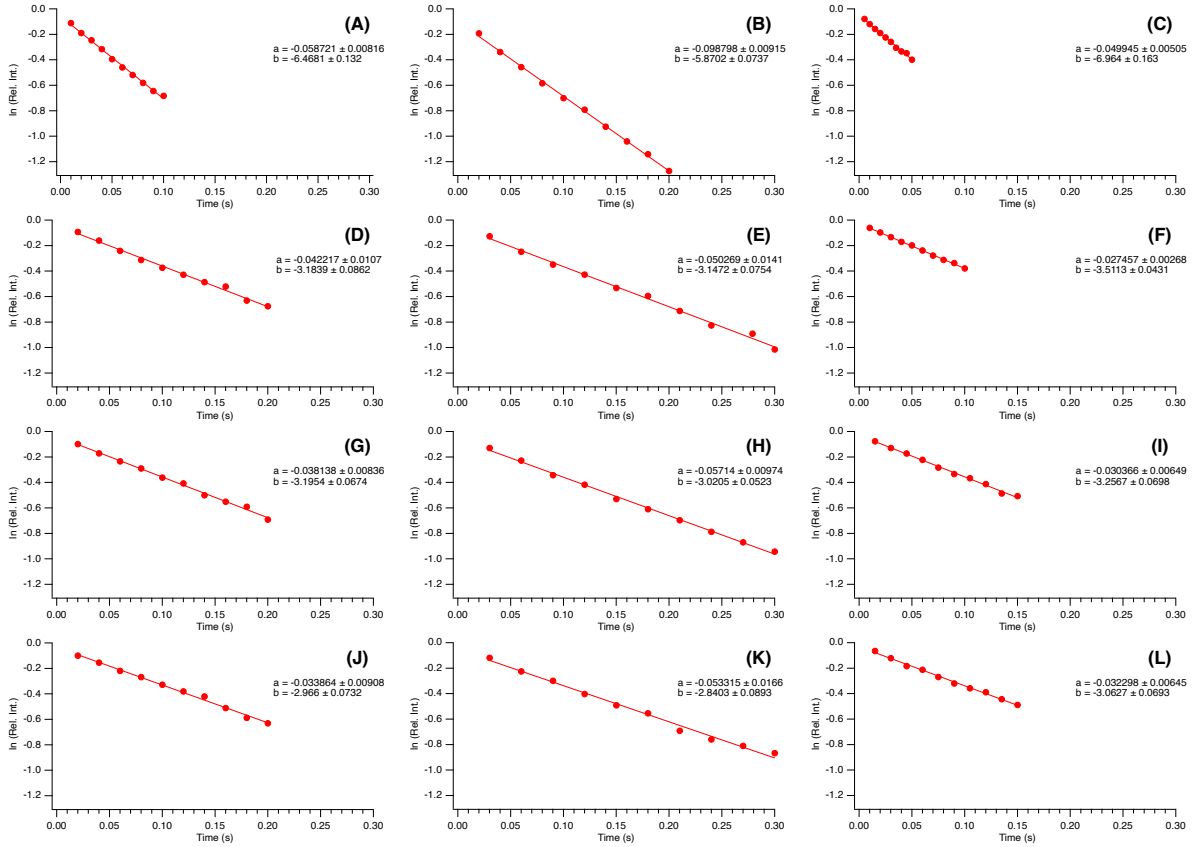

Figure S1 Experimental second order rate constant plots of the ion-molecule reaction (IMR) of Br^- with CH_3I with the following neutral concentrations in the ion trap: *ca.* 2.20 $\times 10^{11}$ molecule per cm^3 (A) – (C), and *ca.* 1.10 $\times 10^{11}$ molecule per cm^3 (D) – (L).

Table S2 Assessment of several commonly used density functionals on the vertical detachment energy (VDE) and adiabatic detachment energy (ADE) of $PhCC^-$. All values are given in eV.

Method	**VDE**	**ADE**
NIPES	3.220(10)	3.220(10)
ωB97X-D/aug-cc-pVTZ	3.10 [3.23]* {3.23}†	3.02 [3.12] {3.14}
M06-2X-D3/‡aug-cc-pVTZ	3.28 [3.22]	3.20 [3.12]
MN15-D3(BJ)/§aug-cc-pVTZ	3.16 [3.22]	3.08 [3.12]
ωB97X-D/6-311++G**	3.13 [3.22]	3.05 [3.12]

* Values in square parentheses represent single-point energy calculations obtained at the DLPNO-CCSD(T)/aug-cc-pVTZ level of theory.

† Values in curly braces represent single-point energy calculations obtained at the PWPB95-D4/aug-cc-pVQZ level of theory.

‡ M06-2X-D3 reference.[1,2]

§ MN15-D3(BJ) reference.[3-5]

Table S3 Optimized key bond lengths in $PhCC^-$ (Å) computed at different levels of theory.

Method	***d*(C≡C)**	***d*(C-C$_{ipso}$)**	***d*(C=C)**		
ωB97X-D/aug-cc-pVTZ*	1.239	1.418	1.408	1.384	1.390
M06-2X-D3/aug-cc-pVTZ*	1.240	1.420	1.410	1.385	1.391
MN15-D3(BJ)/aug-cc-pVTZ*	1.243	1.419	1.411	1.386	1.392
ωB97X-D/6-311++G***	1.243	1.420	1.412	1.387	1.394
CCSD/6-311+G(2d,p)†	1.249	1.430	1.413	1.393	1.398
B3LYP/6-311+G(2d,p)†	1.244	1.415	1.417	1.387	1.396
PBE0/6-311+G(2d,p)†	1.245	1.413	1.412	1.384	1.392
PBE0/aug-cc-pVTZ†	1.244	1.412	1.412	1.384	1.391
BHLYP/DZP++‡	1.245	1.412	1.422	1.388	1.395
B3LYP/DZP++‡	1.261	1.426	1.424	1.398	1.407
MP2/DZP++‡	1.276	1.424	1.429	1.402	1.408

* Present work

† Selected examples from P. Pichierri, *Chem. Phys. Lett.*, 2008, **454**, 404 – 408.

‡ Selected examples from Sreeruttun *et al., J. Phys. Chem. A*, 2008, **112**, 2838 – 2845.

Table S4 Optimized key bond lengths in $PhCC^{\bullet}$ (Å) computed at different levels of theory.

Method	***d*(C≡C)**	**d(C-C$_{ipso}$)**	***d*(C=C)**		
ωB97X-D/aug-cc-pVTZ*	1.272	1.393	1.413	1.377	1.396
M06-2X-D3/aug-cc-pVTZ*	1.273	1.398	1.411	1.378	1.393
MN15-D3(BJ)/aug-cc-pVTZ*	1.275	1.395	1.414	1.379	1.395
ωB97X-D/6-311++G***†	1.276	1.396	1.416	1.381	1.396
ωB97X-D/6-311G(d,p)‡	1.276	1.397	1.415	1.381	1.395
BHLYP/DZP++§	1.276	1.399	1.415	1.382	1.397
B3LYP/DZP++§	1.290	1.404	1.428	1.391	1.408

* Present work

† Karir *et al.*, *Phys. Chem. Chem. Phys.*, 2024, **26**, 18526 – 18265.

‡ Goettl *et al.*, *J. Phys. Chem. A*, 2023, **127**, 5723 – 5733.

§ Selected examples from Sreeruttun *et al., J. Phys. Chem. A*, 2008, **112**, 2838 – 2845.

Table S5 Orbital energies and calculated vertical detachment energies (VDE) for $PhCC^-$. Values are given in eV.

MO	**Orbital energy (ε_H)**	**Δ**	**VDE_n (calc.)***
HOMO	-3.100	0.000	3.220
HOMO-1	-3.596	0.496	3.716
HOMO-2	-3.702	0.602	3.822
HOMO-3	-5.549	2.448	5.668
HOMO-4	-6.197	3.096	6.316

* The first VDE was aligned with the experimental VDE to allow for better comparison with the higher VDEs which were obtained by adding the experimental BDE to the negative of the orbital energies $| -\varepsilon_H + VDE |$.

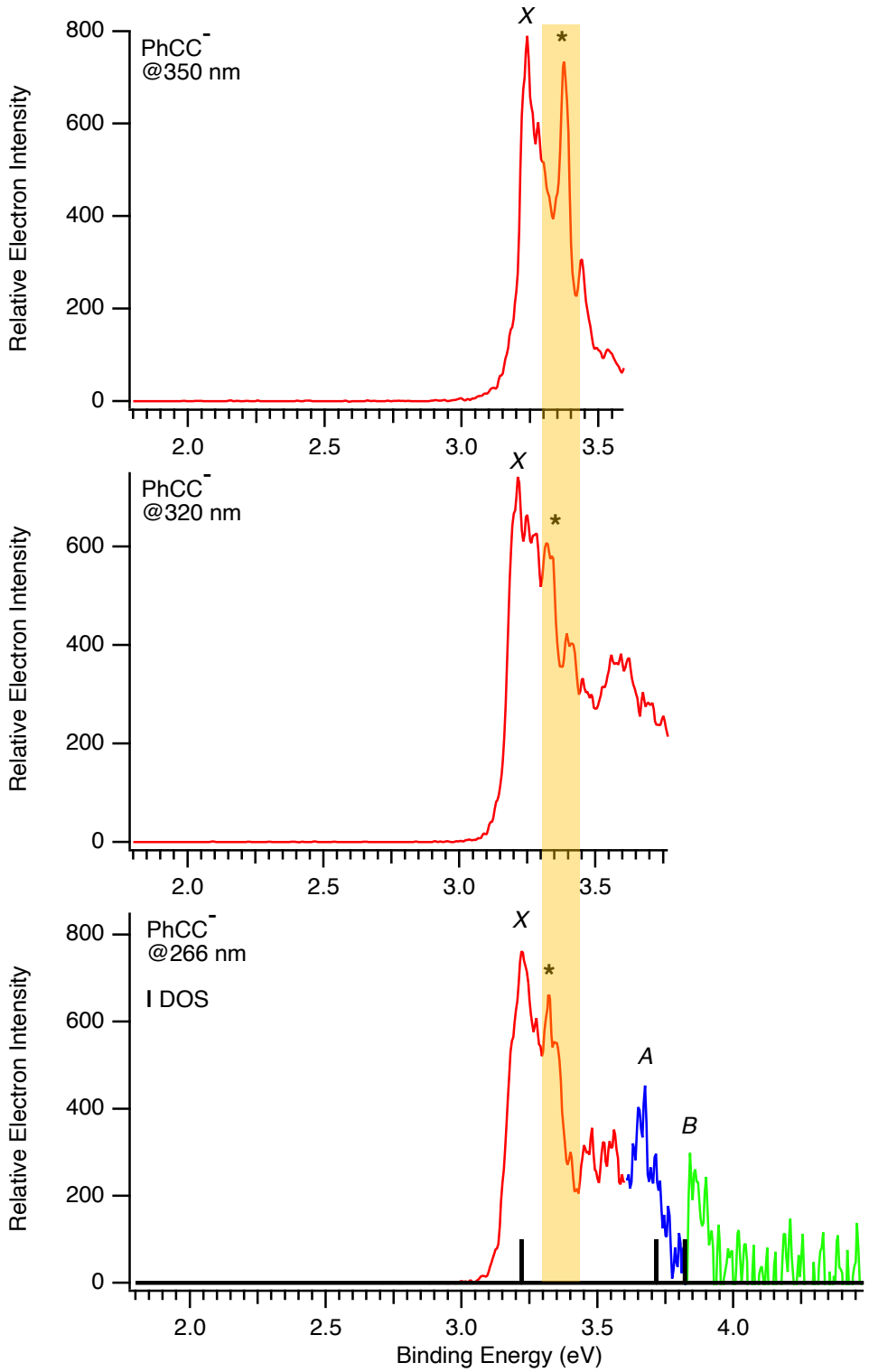

Figure S2 NIPE spectra of $PhCC^-$ obtained at 350 nm (top), 320 nm (middle), and 266 nm (bottom) showing the spectral variation around the band * position, indicative of its resonant detachment feature. The vertical lines (black) are the density-of-states of $PhCC^-$, corroborate *X*, *A*, and *B* bands derived from detaching one electron from HOMO, HOMO-1, and HOMO-2, respectively. Comparison between NIPES spectra at 266 nm (red trace) and computed density-of-states (DOS) stick spectra with the HOMO level shifted to match the *X* band of $PhCC^-$.

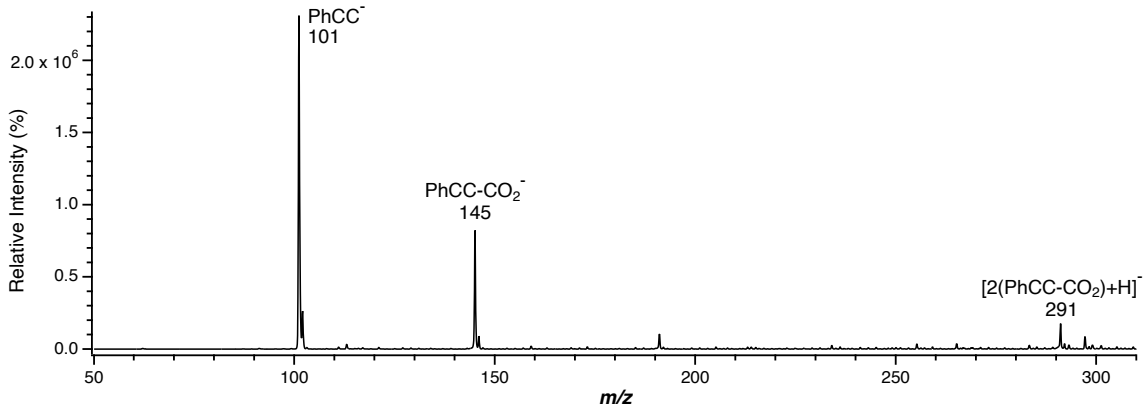

Figure S3 Linear ion trap negative ion mode ESI-MS of phenylpropiolic acid in methanol.

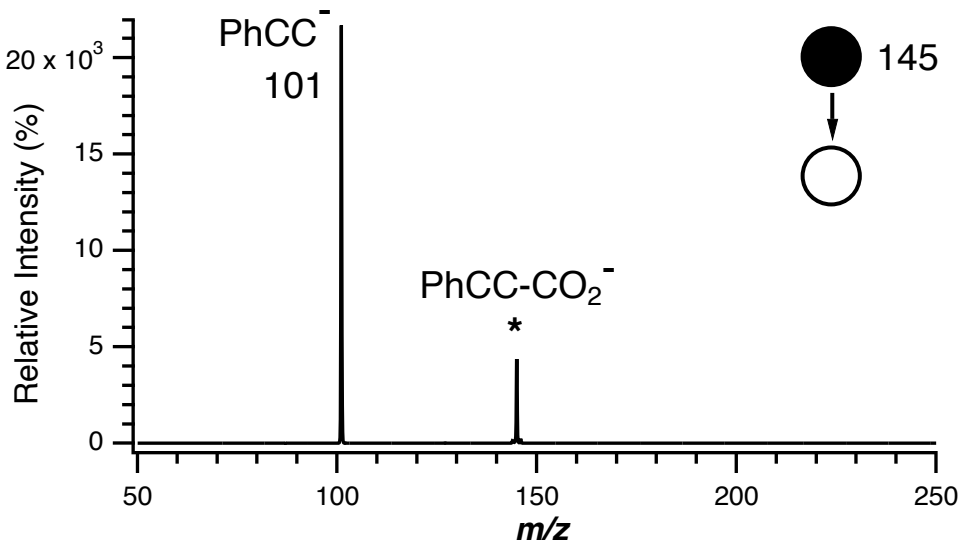

Figure S4 MS^2-CID mass spectrum of phenylpropiolate $PhCC–CO_2^-$ (*m/z* 145) showing the formation of $PhCC^-$ (*m/z* 101) *via* decarboxylation, obtained using a *Q* value of 0.25, an activation time of 10 ms, and at a Normalized Collision Energy (NCE) of 12%. The mass selected precursor ion is denoted by an asterisk (*).

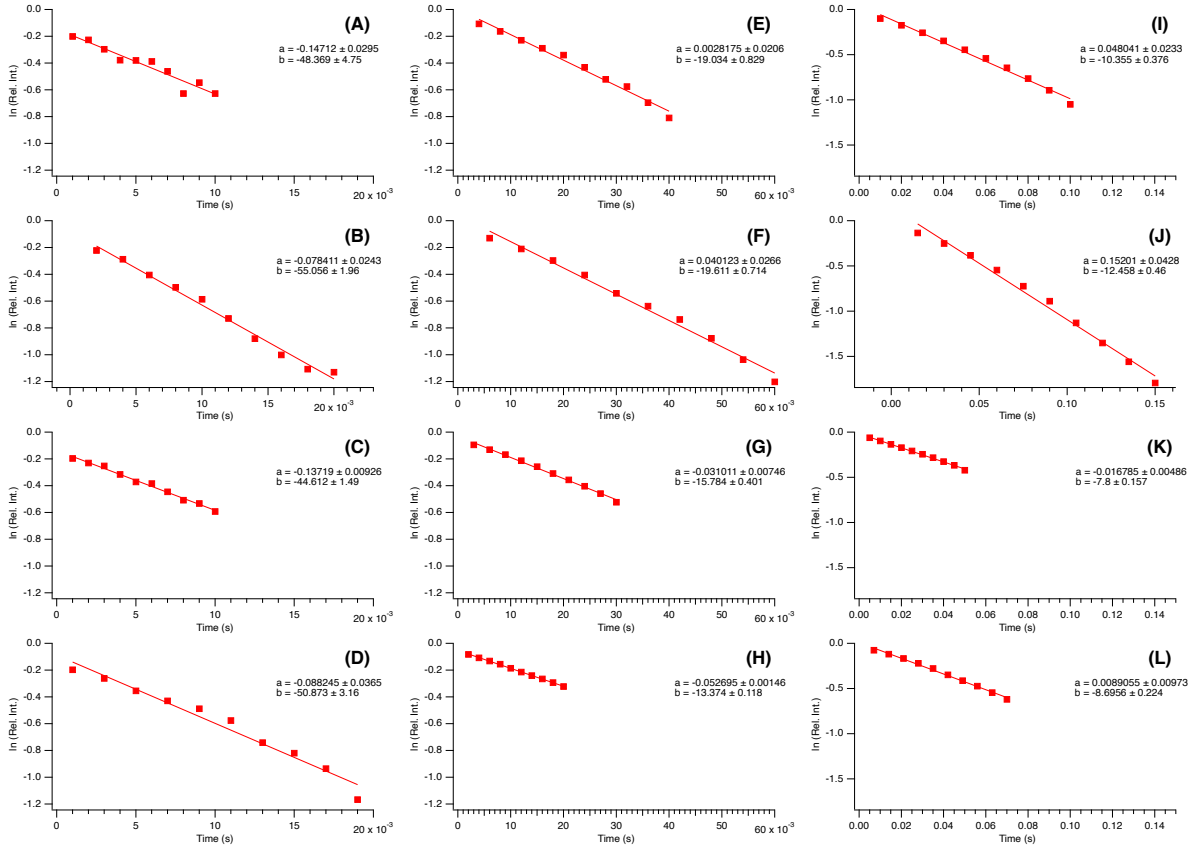

Figure S5 Experimental second order rate constant plots of the ion-molecule reaction (IMR) of $PhCC^-$ with CH_3I with the following neutral concentrations in the ion trap: *ca.* 1.10×10^{11} molecule per cm^3 (A) – (D); *ca.* 4.39×10^{10} molecule per cm^3 (E) – (H), and; *ca.* 2.20×10^{10} molecule per cm^3 (I) – (L).

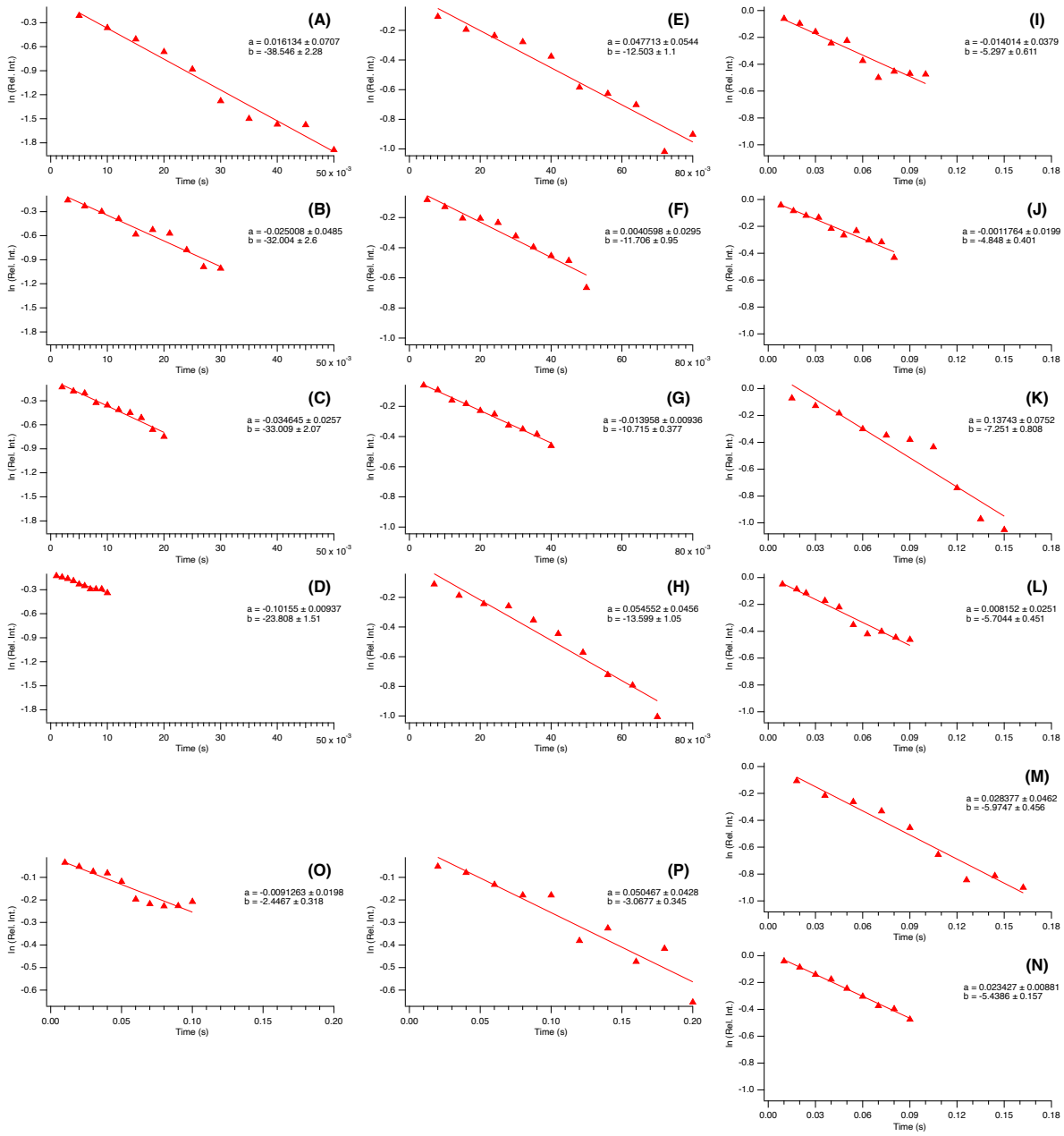

Figure S6 Experimental second order rate constant plots of the ion-molecule reaction (IMR) of $PhCC^-$ with C_3H_5I with the following neutral concentrations in the ion trap: *ca.* 8.13 $\times 10^{10}$ molecule per cm^3 (A) – (D); *ca.* 3.25 $\times 10^{10}$ molecule per cm^3 (E) – (H); *ca.* 1.63 $\times 10^{10}$ molecule per cm^3 (I) – (N), and; *ca.* 8.13 $\times 10^{9}$ molecule per cm^3 (O) – (P).

Table S6 HRMS experiments (Orbitrap Elite ETD linear ion trap mass spectrometer) confirming assignments of key ions.

Ion found in Fig. #	**Ion**	**Exact mass – experimental (*m/z*)**	**Exact mass – calculated (*m/z*)**	**Mass error (ppm)**
5, S3, S4	$PhCC^-$	101.0395	101.0386	8.9
S3, S4	$PhCC–CO_2^-$	145.0293	145.0284	6.2
5	I^-	126.9048	126.9039	7.1

Table S7 Literature rate constants for the ion-molecule reactions between various anions (X^-) and methyl iodide.

X^-	PA(X^-)*	k_{expt} ($\times 10^{-10}$ cm^3 molecule^{-1} s^{-1})†	ϕ
H_2N^-	403.44 ± 0.28	31	1.3
HO^-	390.330 ± 0.010	30	1.3
HO_2^-	376.50 ± 0.50	22	1.3
F^-	372 ± 1	26	1.2
$PhCC^-$‡	**370.6 ± 2.3**	**4.29**	**0.37**
H_2NS^-	356.9 ± 3.1	13	0.88
HS^-	351.4 ± 0.7	8.9	0.52
CN^-	351.1 ± 2.1	1.8	0.096
NCO^-	344.7 ± 2.1	0.13	0.0084
N_3^-	344 ± 3	1.3	0.084
NSO^-	344 ± 5[6]	0.28	0.021
Cl^-	333.6 ± 2.1	2.1	0.13
NCS^-	328.6 ± 5.1	<0.002	<0.00015
Br^-	323.4 ± 2.1	0.33	0.027

* Values obtained from NIST Chemistry WebBook, unless otherwise noted.
† Rate coefficients from Bierbaum *et al.*[6]
‡ Present work, see main text.

Table S8 Comparison of literature rate constants for the ion-molecule reactions between fluoride (F^-) and acetylide (HCC^-) with methyl halides (CH_3Cl and CH_3Br).

X^-	CH_3Y	k_{expt} ($\times 10^{-10}$ cm^3 molecule^{-1} s^{-1})†	ϕ	Method*
F^-	CH_3Br	12	0.59	FA[7]
		6	0.28	ICR[8]
		12	n/a	FA[9]
		12	0.51	ICR[10]
HCC^-	CH_3Br	5.2	0.26	FA[7]
		4.3	0.20	ICR[10]
		3.1	0.16	ICR[11]
F^-	CH_3Cl	19	0.83	FA[7]
		8	0.35	ICR[8]
		5.84	0.23	ICR[12]
		19	n/a	FA[9]
		8.3	0.35	ICR[10]
		5.8	0.25	ICR[11]
HCC^-	CH_3Cl	1.3	0.062	FA[7]
		0.87	0.041	ICR[10]
		0.52	0.024	ICR[11]

* FA: Flowing afterglow; ICR: Ion cyclotron resonance

Table S9 DFT energies (PWPB95-D4/aug-cc-pVQZ(PP)//ωB97X-D/aug-cc-pVTZ(PP)) relative to the reactants for the potential energy surface of $PhCC^-$ (**1**) and CH_3I. Values in parentheses are the energies at the ωB97X-D/aug-cc-pVTZ(PP) level of theory.

Species	ΔH^0	ΔH^{298}	ΔG
1 + CH_3I	0.0 (0.0)	0.0 (0.0)	0.0 (0.0)
IMC1	-9.2 (-9.7)	-9.8 (-8.8)	-3.0 (-2.7)
TS1	-8.2 (-6.1)	-7.9 (-5.8)	0.2 (2.3)
IMC2	-69.6 (-71.8)	-69.2 (-71.5)	-61.9 (-64.1)
PhCC-CH_3 + I^-	-63.5 (-65.8)	-63.3 (-65.6)	-60.6 (-62.9)

Table S10 DFT energies (PWPB95-D4/aug-cc-pVQZ(PP)//ωB97X-D/aug-cc-pVTZ(PP)) relative to the reactants for the potential energy surface of $PhCC^-$ (**1**) and C_3H_5I. Values in parentheses are the energies at the ωB97X-D/aug-cc-pVTZ(PP) level of theory.

Species	ΔH^0	ΔH^{298}	ΔG
1 + C_3H_5I	0.0 (0.0)	0.0 (0.0)	0.0 (0.0)
IMC3	-11.6 (-11.9)	-10.9 (-11.2)	-3.0 (-3.2)
TS2	-7.1 (-4.6)	-6.6 (-4.0)	1.4 (4.0)
IMC4*	-68.9 (-71.4)	-68.6 (-71.1)	-60.8 (-63.3)
IMC3′	-11.5 (-12.0)	-10.9 (-11.4)	-2.2 (-2.7)
TS2′	-3.0 (-0.6)	-2.8 (-0.4)	5.2 (7.6)
PhCC-C_3H_5 + I^-	-61.2 (-63.7)	-60.9 (-63.5)	-58.1 (-60.7)

* As mentioned in the main text, the IRC calculation from **TS2** and **TS2′** essentially give the same structure **IMC4** thus only one entry is presented in this table. For the final structures from the individual IRC calculations, see the supplementary xyz file.

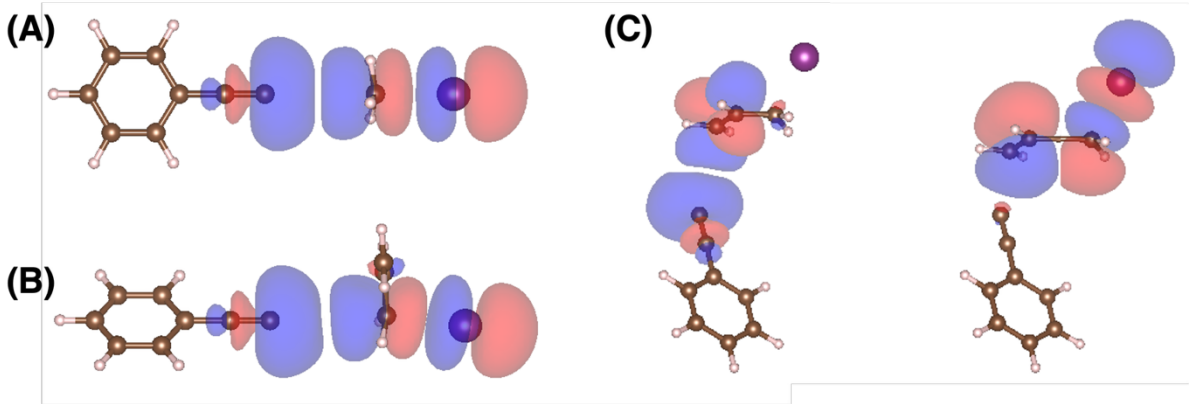

Figure S7 Natural bond order (NBO) interactions in: (A) **TS1**; (B) **TS2**, and; (C) **TS3**, visualized at an isosurface value of 0.02 au.

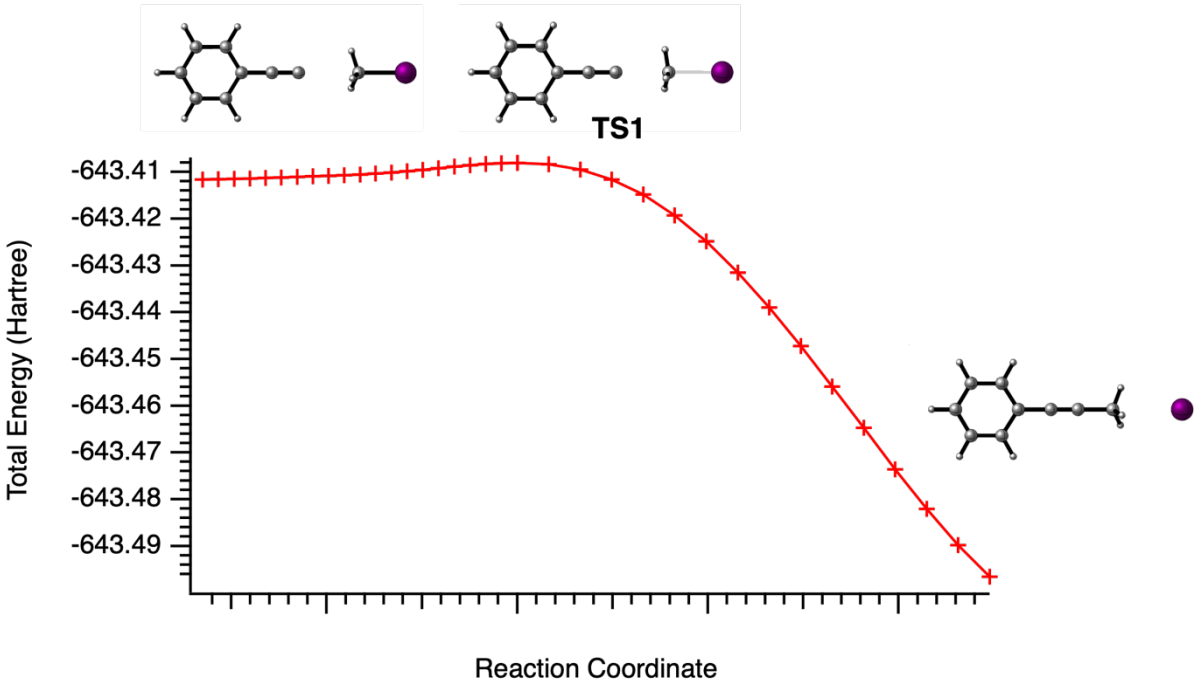

Figure S8 Intrinsic Reaction Coordinate (IRC) calculations for the IMR between $PhCC^-$ (**1**) and CH_3I corresponding to the S_N2 pathway *via* **TS1** at the ωB97X-D/aug-cc-pVDZ(PP) level of theory. The double-ζ basis set was used here instead of the triple-ζ basis set for computational efficiency, the structures presented on the potential energy surface have been optimized with the aug-cc-pVTZ(PP) basis set.

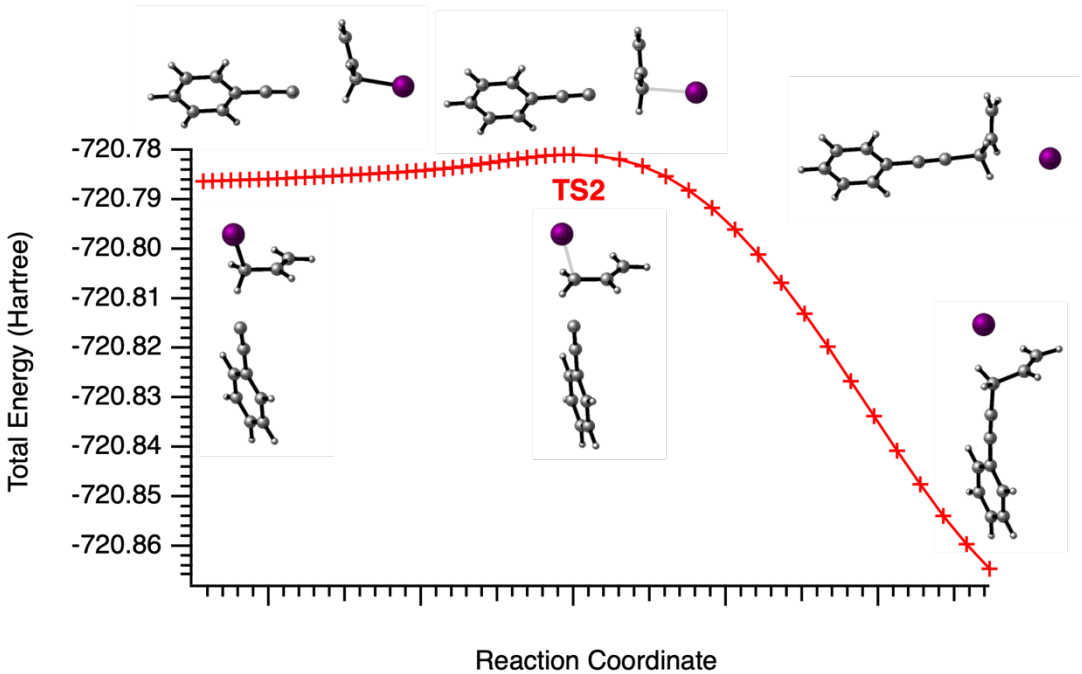

Figure S9 Intrinsic Reaction Coordinate (IRC) calculations for the IMR between $PhCC^-$ (**1**) and C_3H_5I corresponding to the S_N2 pathway *via* **TS2** at the ωB97X-D/aug-cc-pVDZ(PP) level of theory. The structures on the bottom represent an alternate view. The double-ζ basis set was used here instead of the triple-ζ basis set for computational efficiency, the structures presented on the potential energy surface have been optimized with the aug-cc-pVTZ(PP) basis set.

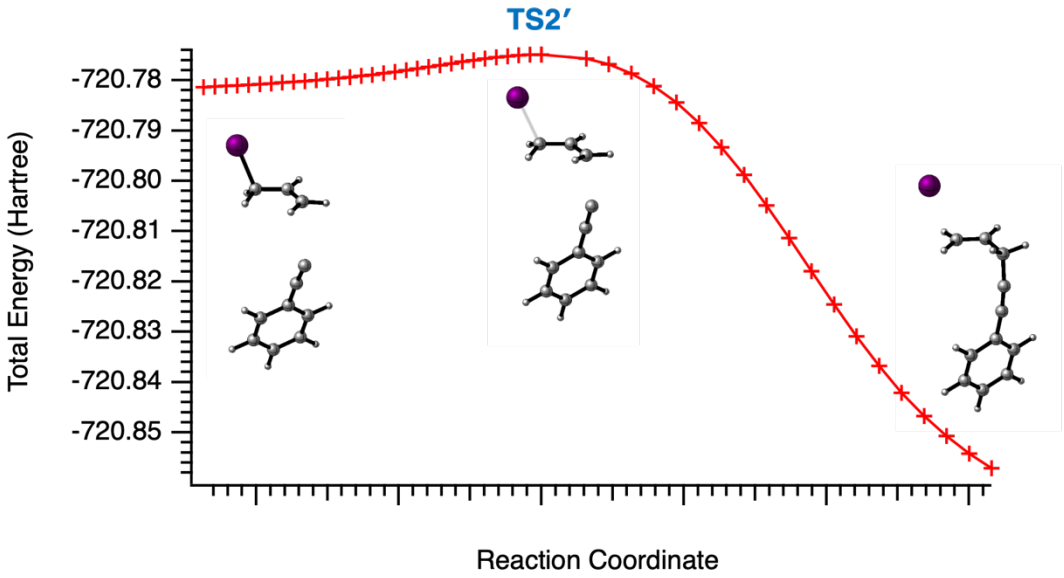

Figure S10 Intrinsic Reaction Coordinate (IRC) calculations for the IMR between $PhCC^-$ (**1**) and C_3H_5I corresponding to the S_N2 pathway *via* **TS2′** at the ωB97X-D/aug-cc-pVDZ(PP) level of theory. The double-ζ basis set was used here instead of the triple-ζ basis set for computational efficiency, the structures presented on the potential energy surface have been optimized with the aug-cc-pVTZ(PP) basis set.

References

1. Y. Zhao and D. G. Truhlar, *Theor. Chem. Acc.*, 2008, **120**, 215-241.
2. S. Grimme, J. Antony, S. Ehrlich and H. Krieg, *J. Chem. Phys.*, 2010, **132**, 154104.
3. H. S. Yu, X. He, S. L. Li and D. G. Truhlar, *Chem. Sci.*, 2016, **7**, 6278-6279.
4. H. S. Yu, X. He, S. L. Li and D. G. Truhlar, *Chem. Sci.*, 2016, **7**, 5032-5051.
5. S. Grimme, S. Ehrlich and L. Goerigk, *J. Comput. Chem.*, 2011, **32**, 1456-1465.
6. V. M. Bierbaum, J. J. Grabowski and C. H. DePuy, *J. Phys. Chem.*, 1984, **88**, 1389-1393.
7. K. Tanaka, G. I. Mackay, J. D. Payzant and D. K. Bohme, *Can. J. Chem.*, 1976, **54**, 1643-1659.
8. W. N. Olmstead and J. I. Brauman, *J. Am. Chem. Soc.*, 1977, **99**, 4219-4228.
9. D. K. Bohme and A. B. Raksit, *Can. J. Chem.*, 1985, **63**, 3007-3011.
10. S. Ingemann and N. M. M. Nibbering, *Can. J. Chem.*, 1984, **62**, 2273-2281.
11. M. J. Pellerite and J. I. Brauman, *J. Am. Chem. Soc.*, 1983, **105**, 2672-2680.
12. M. J. Pellerite and J. I. Brauman, *J. Am. Chem. Soc.*, 1980, **102**, 5993-5999.